Monatshefte für Chemie - Chemical Monthly
https://doi.org/10.1007/s00706-021-02779-7

ORIGINAL PAPER

New 4,5-diphenylimidazole-acetamide-1,2,3-triazole hybrids as potent α-glucosidase inhibitors: synthesis, in vitro and in silico enzymatic and toxicity evaluations

Nima Sepehri[1] · Homa Azizian[2] · Reza Ghadimi[3] · Fahimeh Abedinifar[4] · Somayeh Mojtabavi[5] · Mohammad Ali Faramarzi[5] · Ali Akbar Moghadamnia[6] · Ebrahim Zabihi[6] · Gholamhossein Mohebbi[7] · Bagher Larijani[4] · Haleh Hamedifar[8] · Maryam Mohammadi-Khanaposhtani[6] · Mohammad Mahdavi[4]

Received: 9 January 2021 / Accepted: 29 April 2021

Abstract

Herein, a new series of 4,5-diphenylimidazole-acetamide-1,2,3-triazole hybrids as potent α-glucosidase inhibitors was designed and synthesized. All the synthesized compounds exhibited excellent inhibition potencies (IC_{50} values = 55.6–149.2 µM) against α-glucosidase when compared with the standard inhibitor acarbose (IC_{50} = 750.0 µM). Among the newly synthesized compounds, 4-methyl, 4-methoxy, and 2,3-dichloro derivatives exhibited the highest anti-α-glucosidase activities and were also non-cytotoxic against human normal dermal fibroblast cells. In silico druglikeness, ADME, and toxicity studies of these compounds were performed and obtained results were compared with acarbose. All the synthesized compounds were also inactive against α-amylase in comparison to acarbose. Kinetic study of the most potent compound, 4-methyl derivative, against α-glucosidase demonstrated that this compound is a competitive inhibitor. Furthermore, in silicoinduced fit docking and molecular dynamic studies were performed to further investigate the interaction, orientation, and conformation of these compounds over the active site of α-glycosidase.

Graphic abstract

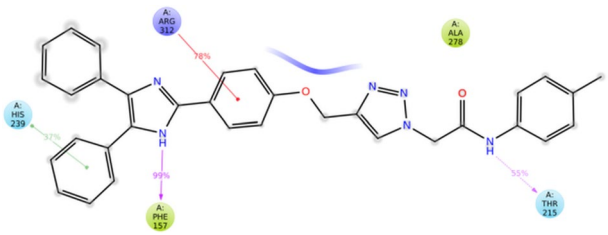

Keywords α-Glucosidase · Kinetic study · Docking study · 4,5-Diphenylimidazole · Acetamide · 1,2,3-Triazole

Introduction

Diabetes mellitus is one of the most common metabolic disorders which lead to increase glucose concentration in the blood because of the defects in insulin production and/or insulin action. High glucose levels over a long time causes serious problems in the vital organs of the human body such as eyes, nerves, and kidneys. The number of diabetic patients is increasing rapidly, and according to the World Health Organization's prediction, by 2030 diabetes will become the seventh leading cause of death. In patients with impaired insulin production, the main treatment is insulin injection, but in patients with insulin dysfunction, the main treatment is suppressing postprandial hyperglycemia by drugs such acarbose and metformin [1, 2]. Acarbose

✉ Maryam Mohammadi-Khanaposhtani
maryammoha@gmail.com

✉ Mohammad Mahdavi
momahdavi@tums.ac.ir

Extended author information available on the last page of the article

Published online: 05 June 2021

inhibited the intestinal α-glucosidase, which is responsible for the release of glucose from carbohydrates (oligosaccharides and disaccharides) into the bloodstream [3]. In addition to α-glucosidase, acarbose also inhibits pancreatic α-amylase that is other important carbohydrate-hydrolyzing enzyme [4, 5]. This enzyme is responsible for convert polysaccharides to oligosaccharides and disaccharides. It is well documented that inhibition of α-amylase increased secretion of undigested polysaccharides to long intestine and led to gastrointestinal side effects such as flatulence, diarrhea, abdominal discomfort, pain, and bloating [6]. On the other hand, in addition to diabetes, inhibition of α-glucosidase can be useful in the other carbohydrate mediated diseases such as cancer and viral infections [7, 8].

4,5-Diarylimidazoles are found in many biological active compounds with anticancer, anti-cyclooxygenase-2, anti-bacterial, and anti-inflammatory activities [9–12]. Furthermore, several 4,5-diarylimidazole derivatives with anti-α-glucosidase activity have been reported (Fig. 1) [13–15]. For example, 4,5-diphenylimidazole-1,2,3-triazole derivatives **A** exhibited high inhibitory activities against α-glucosidase (IC_{50} values = 90.4–246.7 µM comparing with acarbose IC_{50} = 750.0 µM) (Fig. 1) [15]. One of the other important scaffolds for design of new hybrid molecules with various biological activities is 1,2,3-triazole ring [16]. This ring observed in the potent α-glucosidase inhibitors such as benzimidazole-acetamid-1,2,3-triazole derivatives **B** (IC_{50} values = 25.2–176.5 µM comparing with acarbose IC_{50} = 750.0 µM) (Fig. 2) [17, 18]. Because of the presence of 4,5-diphenylimidazole, acetamid-1,2,3-triazole moieties in the potent α-glucosidase inhibitors **A** and **B**, herein, we decided to design and synthesize of 4,5-diphenylimidazole-acetamide-1,2,3-triazole derivatives **C** as new α-glucosidase inhibitors (Fig. 2). To evaluate of interactions of these compounds with α-glucosidase, kinetic, docking, and molecular dynamic studies of these compounds were also performed. Moreover, in vitro cytotoxic effects of the synthesized compounds against the normal human cell line was determined. Furthermore, druglikeness, ADME, and toxicity of these new compounds were also predicted by in silico studies.

Results and discussion

Chemistry

The synthetic route for 4,5-diphenylimidazole-acetamide-1,2,3-triazole hybrids **9a**–**9m** has been depicted in Scheme 1. It was started from the reaction of 4-(prop-2-ynyloxy) benzaldehyde (**1**), benzil (**2**), and ammonium acetate (**3**) in DMF at reflux for 1 h to give 4,5-diphenyl-2-[4-(prop-2-ynyloxy)phenyl]-1*H*-imidazole (**4**). On the other hand, reaction between aniline derivatives **5a**–**5m** and chloroacetyl chloride (**6**) in DMF at room temperature for 30 min let to produce 2-chloro-*N*-phenylacetamide derivatives **7a**–**7m**. Then, the latter compounds and sodium azide reacted in the presence of Et_3N in the mixture of H_2O/*t*-BuOH at room temperature for 1 h to give in situ azide derivatives **8a**–**8m**. Finally, mixture of 4,5-diphenyl-2-[4-(prop-2-ynyloxy) phenyl]-1*H*-imidazole, $CuSO_4$, and sodium ascorbate was added to the freshly prepared azide derivatives **8a**–**8m** and the reaction was continued at room temperature for 18–22 h to give the corresponding products **9a**–**9m**.

In vitro α-glucosidase inhibitory activity

Anti-α-glucosidase activity of the synthesized 4,5-diphenylimidazole-acetamide-1,2,3-triazole hybrids **9a-9m** was determined in vitro against yeast α-glucosidase (*Saccharomyces cerevisiae*, EC 3.2.1.20) and compared with acarbose as standard inhibitor [19]. The obtained result demonstrated that all the compounds **9a**–**9m** are more potent than acarbose (IC_{50} = 750.0 ± 12.5 µM) and among them, the most

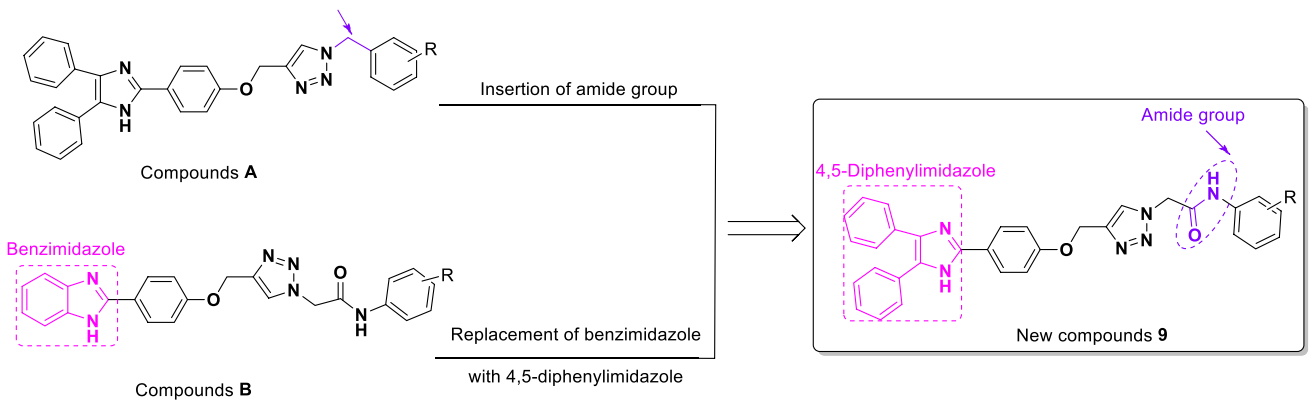

Fig. 1 Design strategy for new 4,5-diphenylimidazole-acetamide-1,2,3-triazole derivatives **9**

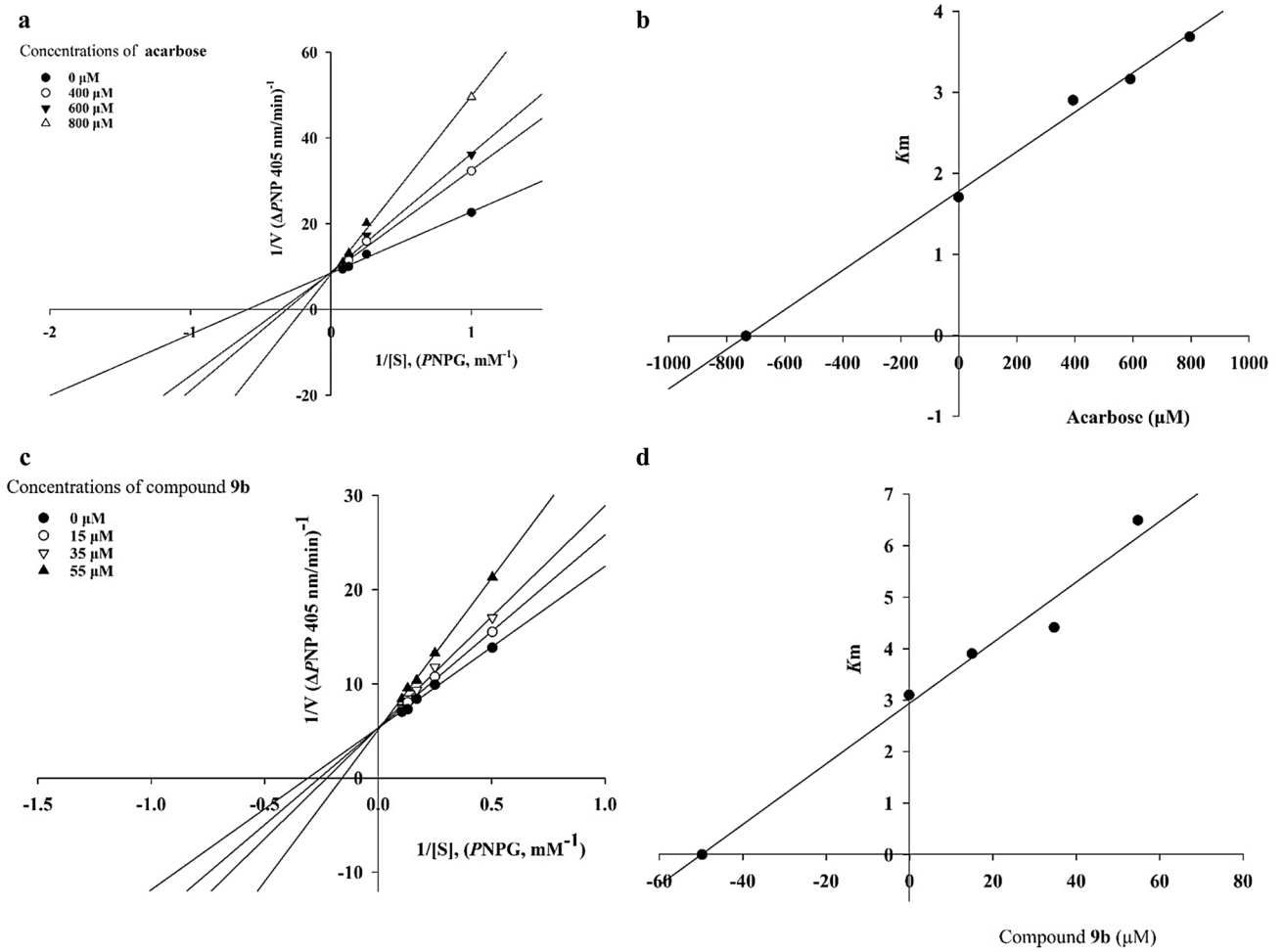

Fig. 2 Kinetics of α-gluosidase inhibition by acarbose and compound **9b**. **a** and **c** Lineweaver–Burk plot in the absence and presence of different concentrations of acarbose and compound **9b**, respectively; **b** and **d** the secondary plot between K_m and various concentrations of acarbose and compound **9b**, respectively

potent compounds were compounds **9b**, **9d**, and **9h** with IC_{50} values 55.6 ± 0.4, 66.7 ± 0.6, and 78.7 ± 0.7 µM, respectively. Moreover, the remaining compounds with the IC_{50} values ranging from 87.7 ± 0.8 to 149.2 ± 1.5 µM exhibited α-glucosidase inhibitory activities around 8.6-5 folds more than acarbose.

To optimize the anti-α-glucosidase activity, the substituent on the phenyl ring of *N*-phenylacetamide moiety was altered. Among the *N*-phenylacetamide derivatives **9a**–**9m**, the most potent compound was 4-methyl derivative **9b**. Removing the methyl substituent or replace it with methoxy or phenoxy substituents, led to a slightly decrease in the

Scheme 1

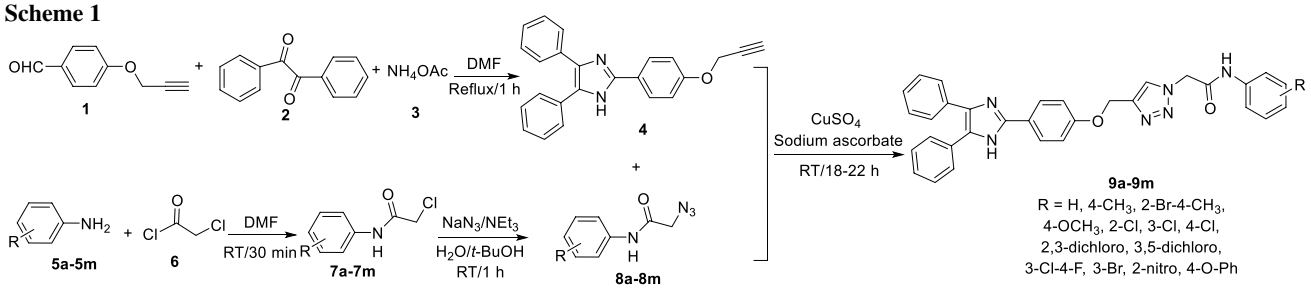

inhibitory activity as observed in the compounds **9a**, **9d**, and **9m,** respectively. As can be seen in Table 1, adding a bromine atom to 4-methylphenyl group dramatically decreased inhibitory activity (compound **9b** vs. compound **9c**).

Among the chloro-substituted derivatives **9e**–**9j**, compound **9h** with 2,3-dichlorophenyl moiety was the most potent compound. Removing the 3-chloro substituent, as in compound **9e**, led to slightly decrease in the inhibitory activity while movement of 2-chloro to 5-position, as in compound **9i**, led to a significant decrease in the inhibitory activity. In addition, inhibitory activity of the compounds **9e**–**9g** with a chloro substituent, demonstrated that translocation of chlorine atom on the phenyl group of *N*-phenylacetamide moiety had significant effect on α-glucosidase inhibitory activity, and 2-chloro was preferred [order of inhibitory activity: 2-Cl (compound **9e**) > 3-Cl (compound **9f**) > 4-Cl (compound **9g**)]. Replacement of chlorine atom at 3-position with bromine atom (compound **9k**) or 2-position with nitro group (compound **9l**) increased α-glucosidase inhibition. Moreover, adding a fluorine atom to 4-position of 3-chlorophenyl derivative **9f** led to a significant decrease in the inhibitory activity as observed in the compound **9j**.

Table 1 α-Glucosidase and α-amylase inhibitory activities of imidazole-acetamide-1,2,3-triazoles derivatives **9a**–**9m**

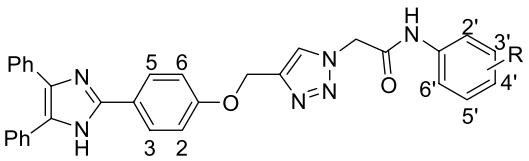

Compound	R	IC_{50}/μM	
		α-glucosidase	α-amylase
9a	H	87.7 ± 0.8	> 200
9b	4-CH_3	55.6 ± 0.4	> 200
9c	2-Br-4-CH_3	129.3 ± 1.3	> 200
9d	4-OCH_3	66.7 ± 0.6	> 200
9e	2-Cl	107.6 ± 1.1	> 200
9f	3-Cl	116.6 ± 1.2	> 200
9g	4-Cl	125.2 ± 1.3	> 200
9h	2,3-dichloro	78.7 ± 0.7	> 200
9i	3,5-dichloro	134.5 ± 1.4	> 200
9j	3-Cl-4-F	149.2 ± 1.5	> 200
9k	3-Br	98.2 ± 1.0	> 200
9l	2-Nitro	94.7 ± 0.9	> 200
9m	4-O-Ph	83.7 ± 0.8	> 200
Acarbose	–	750.0 ± 12.5	108 ± 0.71

The comparison of IC_{50} values of the new 4,5-diphenylimidazole-acetamide-1,2,3-triazole derivatives **9** with their corresponding analogs of 4,5-diphenylimidazole-1,2,3-triazole series **A** revealed that presence of acetamid unit increased α-glucosidase inhibitory activity (Scheme 2) [15]. Therefore, it seems that our strategy to replacement of benzyl moieties of compounds **A** with *N*-phenylacetamide moieties led to increase in inhibitory activity against α-glucosidase.

In contrast, this comparison between new compounds **9** and reported benzimidazole-acetamid-1,2,3-triazole derivatives **B** revealed that, with the exception of 4-methoxy derivative of 4,5-diphenylimidazole series, benzimidazole derivatives were more potent than their analogs of 4,5-diphenylimidazole series (Scheme 3) [17].

α-Amylase inhibition assay of the synthesized compounds was also performed and obtained results demonstrated that all new compounds **9a**–**9m** were inactive against α-amylase (IC_{50} > 200 μM) when compared with standard inhibitor acarbose (IC_{50} = 108 ± 0.71 μM) [19].

Kinetic study

To determine the interaction type of the synthesized compounds with α-glucosidase and to compare them with

Scheme 2

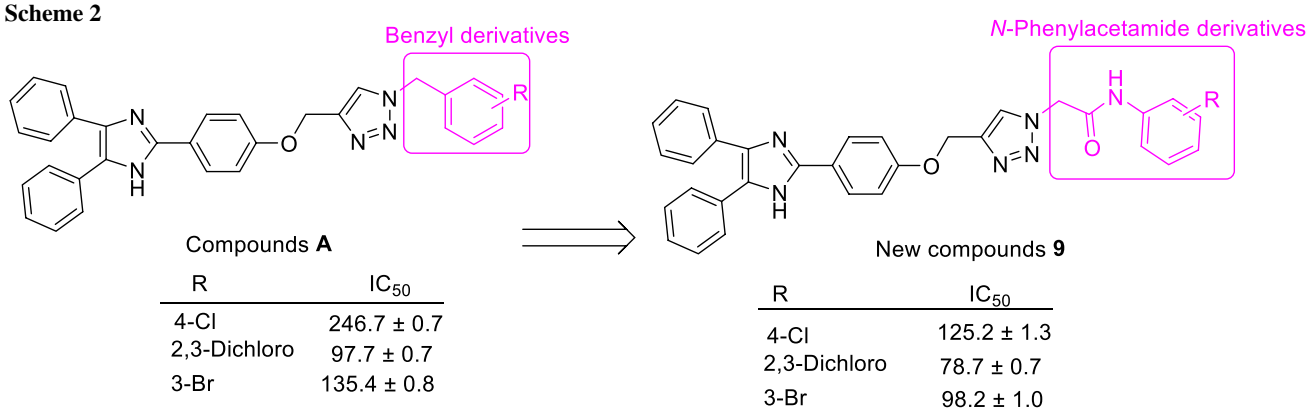

Scheme 3

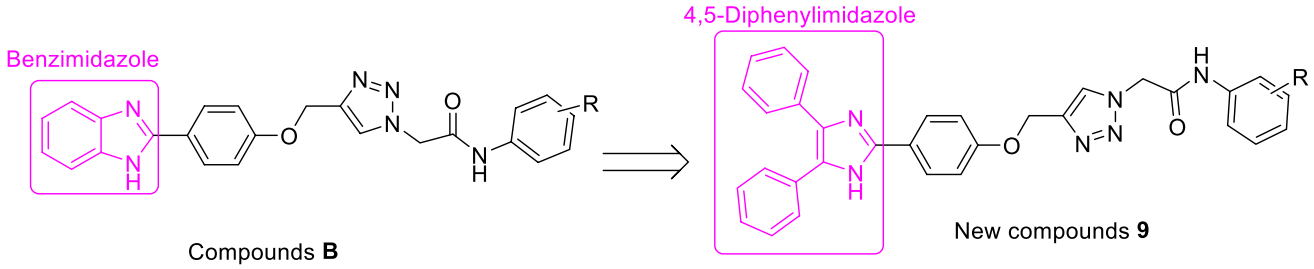

Compounds **B**

R	IC_{50}
H	51.5 ± 1.8
4-Me	43.1 ± 1.5
4-Methoxy	112.5 ± 5.3
2-Cl	70.6 ± 2.6
2,3-Dichloro	56.6 ± 2.1
3-Br	85.2 ± 2.8
2-Nitro	35.0 ± 1.0

R	IC_{50}
H	87.7 ± 0.8
4-Me	55.6 ± 0.4
4-Methoxy	66.7 ± 0.6
2-Cl	107.6 ± 1.1
2,3-Dichloro	78.7 ± 0.7
3-Br	98.2 ± 1.0
2-Nitro	94.7 ± 0.9

standard drug, kinetic studies was performed on the acarbose and the most active compound **9b** [20]. The type of inhibition these compounds and their inhibitory constant were indicated by Lineweaver–Burk plots and the secondary replot of these plots. As shown in Fig. 2a, c, with increasing concentration of acarbose and compound **9b**, V_{max} values were not affected, while the K_m values increased. Therefore, the latter compounds are competitive inhibitors against α-glucosidase. K_i values of acarbose and compound **9b** were 737 and 50 µM, respectively (Fig. 2b, d).

Molecular docking study

Molecular docking study was carried out to evaluate the interaction modes of the newly synthesized compounds **9a**–**9m** in the modeled α-glycosidase [21–26]. The location and residue specification of the modeled α-glycosidase active site is shown in Fig. 3a. According to Yamamoto et al. investigation, the α-glycosidase pocket shape active site located at the interface of domain A and B, which contain conserve residues around the substrate-binding site [27]. There are three conserve acidic residues including Asp214 (Asp215), Asp349 (Asp352), and Glu277 (Glu276), which have the

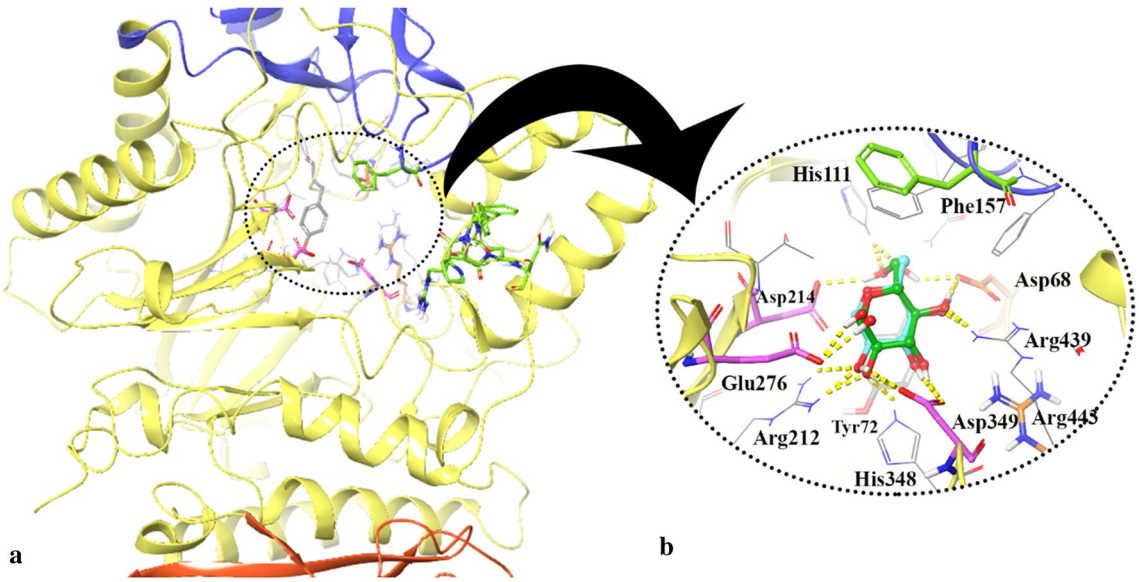

Fig. 3 Representation of α-glycosidase active site. **a** The environment of α-glycosidase active site located at the interface of domain A and B. Domain A, B, and C are colored in yellow, blue, and red, respectively. **b** Close-up representation of active site, the modeled α-D-glucose and the corresponding re-docked form represented in green and cyan color, respectively

catalytic role [28, 29]. His279 (His280), Phe157 (Tyr158), and the loop consisting of residues 310–315 located at the entrance of the active site, while Tyr72 situated at the bottom of the active site. In addition, Asp68 (Asp69) and Arg443 (Arg442) placed at the wall of the active site which have the role in recognition of non-reducing end of the glucose (numbering in the parenthesis indicate the residue numbering according to the isomaltase structure). Finally, residues including Arg439, His111, His348, Arg212, and Gln181 are the residues around the substrate-binding pocket.

The reliability of the applied docking protocol was assessed by re-docking of α-D-glucose into the active site of the α-glucosidase. The key characteristic of a good docking program is its ability to reproduce the actual binding modes of ligands. To test this, α-D-glucose taken out of the modeled protein–ligand complex and re-docked into its binding site. The docked binding mode is then compared with the modeled binding mode, and the RMSD is calculated; successful binding mode prediction is considered if the RMSD is below a certain value (usually < 2.0 Å). Figure 3b shows the superimposed structures between the docked and the modeled α-D-glucose over α-glucosidase, which has RMSD acceptable (RMSD value = 0.3 Å). According to Fig. 3b, the docked glucose molecule is bound at the bottom of the active site pocket by ten hydrogen bonds and it stacks against Tyr72.

After confirmation of modeled α-glycosidase, the top scoring pose of all the title compounds inside the active site was analyzed. Figure 4 represents that the synthesized compounds have two different fitting-in conformers. Both of the conformers are in U-shape structure but have different orientations inside the active site. The first one is related to the compounds **9b**, **9d**, **9k**, and **9h** in which the 4,5-diphenyl-1*H*-imidazol-phenoxy moiety pointed to the mouth of the active site in the manner that 4,5-diphenyl rings stacked between the two loops at the large hydrophobic entrance of the active site; one from domain A (in yellow) and the other one from domain B (in blue). In addition, the 1,2,3-triazol ring and the *N*-phenylacetamide moiety positioned at the bottom of the U conformer and along domains I and II, respectively (Fig. 4a). Figure 4b shows the horizontal U-shape orientation of compounds **9c**, **9f**, **9i**, **9e**, **9g**, **9l** in to the active site in which the 4,5-diphenyl-1*H*-imidazol-phenoxy moiety and *N*-phenylacetamide moiety at the mouth of U structure pointed toward the conserved region I and II and the 1,2,3-triazol ring which is at the bottom of the U structure directed toward the active site mouth.

The molecular interactions of the best conformational pose and energy valued docked complex of compounds **9b**, **9d**, and **9h** with higher inhibition activity and compounds **9e**, **9g**, and **9i** with the relative lower inhibition activity illustrated in Fig. 5.

Compounds **9b**, **9d**, and **9h** shows similar orientation and interaction which is matched to the conformation depicted in Fig. 4a. In all the mentioned compounds the rings related to 1*H*-imidazol, 1,2,3-triazol, and the phenoxy moiety stabilized through π-π stacking and T-shape π-π hydrophobic interaction with the side-chain group of Phe157. In addition, the 1*H*-imidazol ring and the phenoxy oxygen atom (O) formed H-bond interaction with the backbone (C=O) of the Phe157 and side chain of Arg439, respectively (Fig. 5a–c). Figure 5d–f provides the interaction details of compounds **9e**, **9g**, and **9i** in which the 1*H*-imidazol moiety stabilized through H-bond and π-π stacking interaction with Tyr313 and Phe311, respectively. Furthermore, the acetamide linker

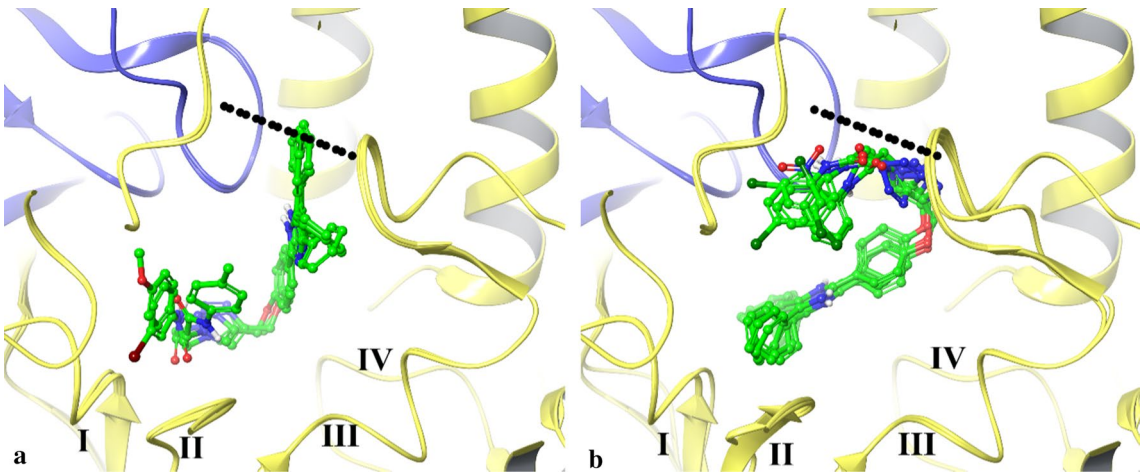

Fig. 4 **a** Docked representation of the compounds **9b**, **9d**, **9k**, and **9h** over the α-glycosidase active site. **b** Docked representation of the compounds **9c**, **9f**, **9i**, **9e**, **9g**, and **9l** over the α-glycosidase active site (domain A and B are colored in yellow and blue, respectively. The docked compounds colored in green. I, II, III, and IV are the four α-glycosidase active site conserved regions and the dash lines depicts the mouth of the active site)

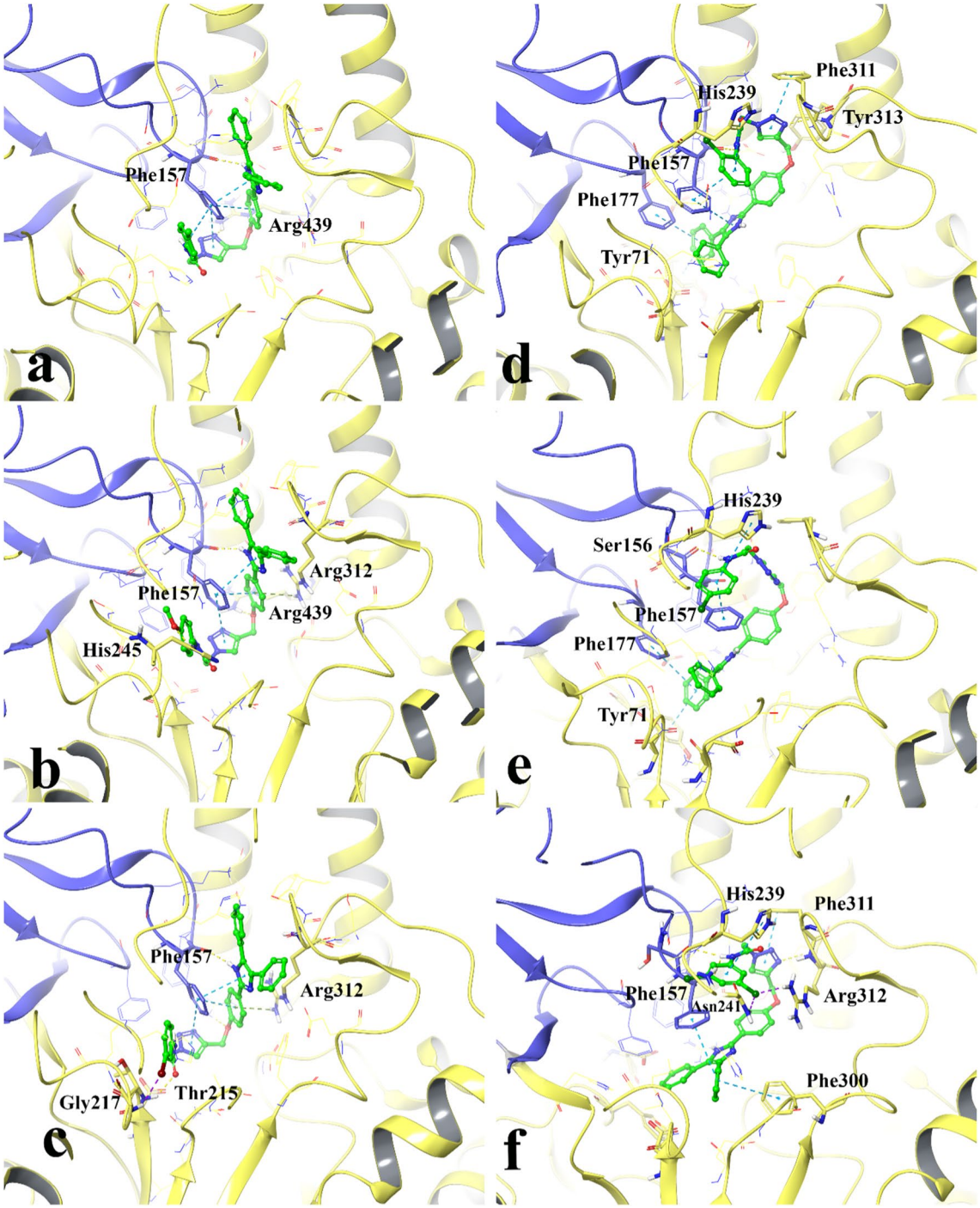

Fig. 5 3D representation of ligand-residue interactions of compounds **9b** (**a**), **9d** (**b**), **9h** (**c**), **9e** (**d**), **9g** (**e**), and **9i** (**f**) over α-glycosidase active site. (Domain A and B are colored in yellow and blue, respectively)

provide H-bond interaction through with the backbone carbonyl group of Ser156 and Phe157, respectively.

Based on the observed IFD result, it can be proposed that our synthetic compounds reside in to the α-glycosidase active site through two different orientations with one of them more corresponding to the higher α-glycosidase inhibition activity. In addition, the presence and the essential interaction role of Phe157 from the B domain side of the active site mouth besides Arg312 from the opposite site over the A domain side of the active site mouth have been identified for compounds stabilization over the α-glycosidase active site.

Molecular dynamic investigation

Additionally, MD simulation was performed to understand the effect of the compound over the enzyme active site [30]. For this purpose, the structural perturbations incurred by the most potent compound **9b** has been investigated through study the RMSD, RMSF, and its effect on the active site environment in comparison to acarbose as α-glycosidase standard inhibitor and the apo enzyme (Fig. 6).

Root mean square deviation (RMSD) of the enzymes' backbone was analyzed over 20 ns MD simulation to study the stability of the protein–ligand complex trajectories. The RMSD value of the apo α-glycosidase depicts broad fluctuations throughout simulation time which is higher than the two enzyme complexes. The RMSD value sharply increased in the first 4 ns and steadily increased up to 16 ns and become more stable for the last 4 ns of simulation time with the value of 2.5 Å. The RMSD value of α-glycosidase complexed with acarbose was stable until 12 ns and slightly increased through the next 4 ns and become steady for the rest of the simulation time with the lower RMSD value of 2 Å.

Comparing the apo enzyme, the RMSD value of α-glycosidase complexed with compound **9b** is highly similar as acarbose bounded state especially for the first 6 ns and slightly increased due to the higher number of ring and flexibility which makes it slightly deviate from the initial structure for the rest of simulation time with the same RMSD as acarbose bounded state (2 Å).

To be brief, the RMSD value of the bounded state enzymes obviously deviated from the apo enzyme at the first time of simulation and obviously decreased as a result of α-glycosidase structural rigidity due to active site bounding state. The RMSD value for the last 5 ns steadily equilibrated around 2 Å and used to investigate the structural specificity of α-glycosidase-ligand complexes.

The flexibility of protein structure can be evaluated through investigating the RMSF value in which evaluate the fluctuation of the protein backbone structure from its average position throughout the whole simulation time. The residue RMSF values of α-glycosidase apo enzyme and the enzyme in bounded state showed that, the apo enzyme (yellow-colored dash box) had higher RMSF fluctuations compared to the glycosidase bound-states (green- and red-colored dash boxes) (Fig. 7a).

According to the result, the mentioned lower RMSF value occurs upon ligand binding to the enzyme, in which residues movement decrease as a result of non-bonding interaction between the ligand and the enzyme active site.

Moreover, Fig. 7a depicts that there are four structural segments which revealed different RMSF pattern upon ligand binding including; B domain loop (pink dash box), the active site lid (pin dash box), A domain and B domain sides of the active site entrance (orange and blue dash boxes).

Based on results shown on Fig. 5a, b, the RMSF value of the B domain loop residues would have decreased in glycosidase/acarbose and compound **9b** bound-state rather than apo enzyme which is due to the presence of non-bonding interaction related to Phe157.

In contrast, although the flexibility of the active site lid was the highest in enzyme acarbose bound state, the mentioned segment flexibility revealed the lowest in glycosidase complexed with compound **9b**. To investigate the proposed reason of the mentioned observation, acarbose and compound **9b** interacted with several residues located both on A and B domain side of the active site mouth (Fig. 7b). Although acarbose showed more interaction with the A side domain of active site entrance (orange dash line

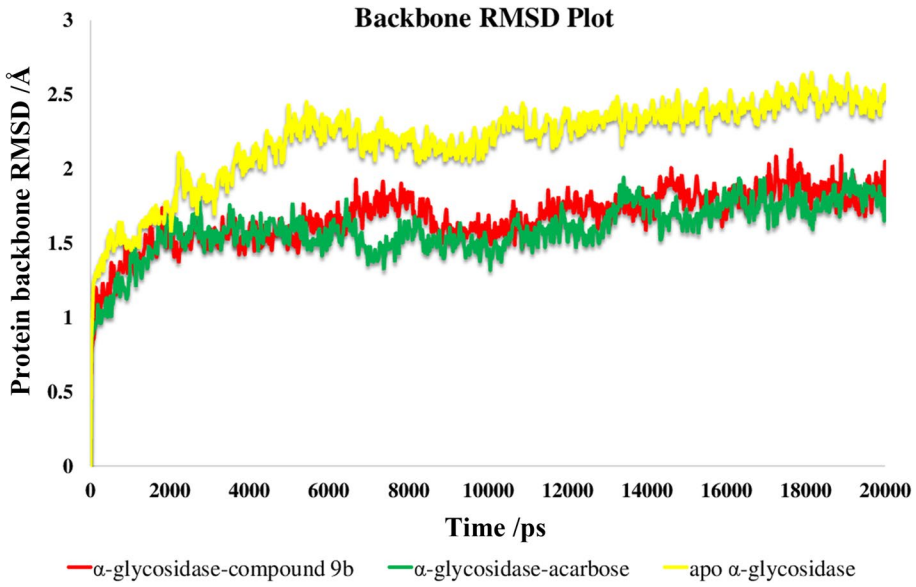

Fig. 6 RMSD of the α-glycosidase backbone in complexed with acarbose (in green), compound **9b** (in red) and the apo enzyme (in yellow) for over 20-ns MD simulation time

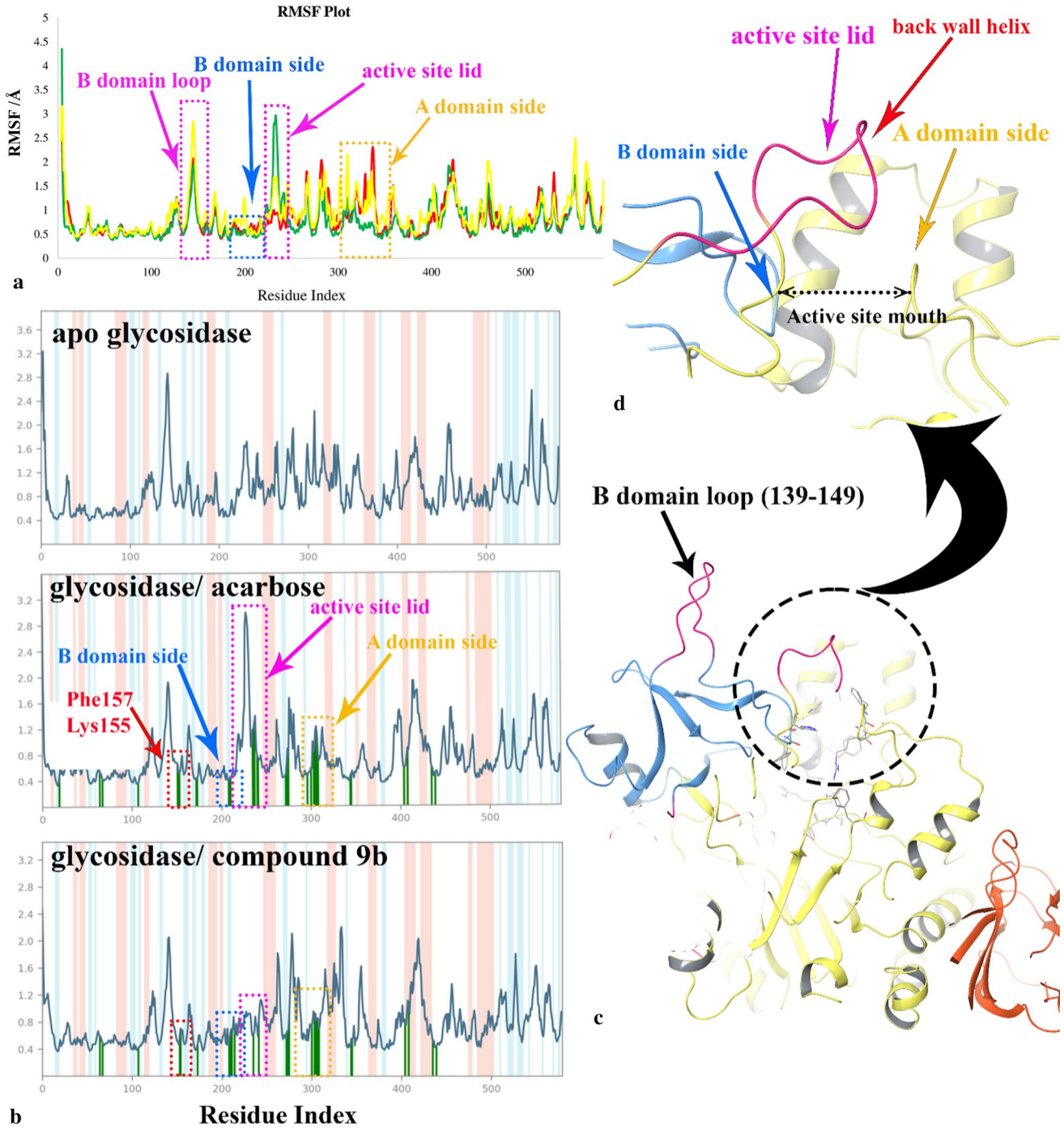

Fig. 7 RMSF plot of the α-glycosidase backbone in complexed with compound **9b** (in red) and acarbose (in green) and the apo enzyme (in yellow) for over 20-ns MD simulation time (**a**). Ligand binding location of glycosidase in bound and unbound-state for over 20 ns MD simulation time (α-helical and ß-strand regions are highlighted in red and blue backgrounds, respectively) (**b**). 3D representation of α-glycosidase structure. Enzyme domain of A, B, and C are colored in yellow, blue, and orange, respectively. The flexible regions correspond to B domain loop and active site lid are colored in pink (**c**). Close-up representation of α-glycosidase active site (**d**)

in glycosidase/acarbose), compound **9b** provided higher number of interactions with the residues of B domain side (blue dash line in glycosidase/compound **9b**). Therefore, it can be proposed that the more ligand interaction with the B domain sides of the active site mouth, the lower RMSF of the active site lid.

Moreover, Fig. 7c, d represents the organization of the α-glycosidase three main domains; A, B, and C along with

the close-up representation of the active site mouth with the corresponding residues of A and B domains at the both sides of active site entrances.

In summary, based on the RMSF plot, acarbose and compound **9b** have almost the same interaction pattern through the whole α-glycosidase structure. The only dissimilarity comes from active site lid flexibility in which we can proposed that compound **9b** along with more interaction over the B domain side of the active site entrance has dominant effect in rigidity of active site lid rather than acarbose which has more interaction with the A domain side of the α-glycosidase active site entrance.

Figure 8 represents the detailed orientation and interactions that occurred more than 30% of the simulation time during the equilibrated phase over α-glycosidase complexed with compound **9b**.

It represents two important structural moieties in stabilizing compound **9b** at the mouth of the active site. The first one is the imidazole ring which interacts with Phe157 located on B domain side of active site entrance through H-bond interactions for the whole simulation time (99%) and the next one, is the central part of the phenoxy ring which interacts with Arg312 located on A domain side through π-cation interaction for 78% of the simulation time. Along to the interactions which stabilized compound **9b** in front of the active site entrance, the acetamide moiety can provide H-bond interaction with Thr215 at the bottom of the active site for about 55% of simulation time.

In addition to the interaction analysis, the Prime/MM-GBSA module was used to estimate the strengths of interactions between the ligand–protein complexes which generated by the clustering method. ΔG_{bind} of α-glycosidase/compound **9b** complex and α-glycosidase/acarbose complex were estimated to be − 349.26 and − 261.63 kJ/mol, respectively, revealing stronger binding interaction of compound **9b** than acarbose which also supported by experimental assay.

Cytotoxicity against normal human cells

Cytotoxicity of the most active compounds **9b**, **9d**, and **9h** was evaluated against human dermal fibroblasts (HDF) cells using by MTT assay [19]. Obtained results revealed that at 80 µM, these compounds were non-cytotoxic against studied cell line.

In silico druglikeness, ADME, and toxicity studies

Druglikeness/ADME/T properties of the compounds **9b**, **9d**, **9h**, and acarbose were evaluated in silico using by online software PreADMET and the predicted results were shown in Table 2 [31]. As can be seen in Table 2, our synthesized compounds and acarbose violated rule of five and are drug like according to MDDR like rule. Acarbose and compounds **9b**, **9d**, and **9h** have poor to medium Caco-2 cell permeability while all studied compounds have low blood brain barrier (BBB) nd skin permeability. On the other hand, compounds **9b**, **9d**, and **9h** have high human oral absorption (HIA) while acarbose does not show HIA. Predicting the toxicity of selected compounds by PreADMET server demonstrated that our synthesized compounds, unlike acarbose, were not mutagenic (Ames test). Furthermore, compounds **9b**, **9d**, and **9h** are medium risk in term of cardiotoxicity while cardiotoxicity of acarbose is ambiguous. Synthesized compounds **9b**, **9d**, and **9h**, unlike acarbose, were not carcinogen on mouse. On the other hand, in term of carcinogenicity on rat, compound **9h** and acarbose were negative.

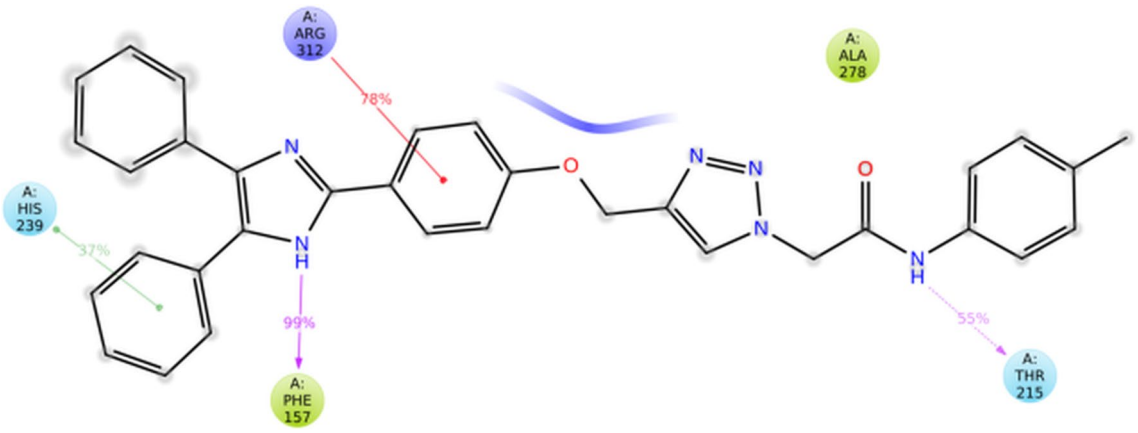

Fig. 8 The detailed orientation and ligand atom interactions that occurred more than 30.0% of the simulation time during the equilibrated phase over α-glycosidase complexed with compound **9b**

Table 2 Druglikeness/ADME/T Profile of the most potent compounds **9b**, **9d**, and **9 h**

Druglikeness/ADME/T[a]	Compound			
	9b	**9d**	**9h**	Acarbose
Rule of five	Violated	Violated	Violated	Violated
MDDR like rule	Drug-like	Drug-like	Drug-like	Drug-like
Caco2	26.095	34.0086	39.3674	9.44448
HIA	95.076467	95.295168	95.513821	0.000000
BBB	2.93397	1.31653	4.71572	0.0271005
Skin permeability	−2.61499	−2.72782	−2.62073	−5.17615
Ames test	Non-mutagen	Non-mutagen	Non-mutagen	Mutagen
hERG inhibition	Medium risk	Medium risk	Medium risk	Ambiguous
Carcino mouse	Negative	Negative	Negative	Positive
Carcino rat	Positive	Positive	Negative	Negative

[a]The recommended ranges for Caco2: < 25 poor, > 500 great, HIA: > 80% is high < 25% is poor, BBB = −3.0–1.2, and Skin_Permeability = −8.0 to −1.0

Conclusion

In conclusion, we presented hybrid structures of 4,5-diphenylimidazole-acetamide-1,2,3-triazole, and acetamide moieties as new α-glucosidase inhibitors. The results of anti-α-glucosidase activity of the synthesized compounds **9a**–**9m** revealed that all these compounds were more potent than standard inhibitor acarbose. Among them, compounds **9b**, **9d**, and **9h** exhibited the highest α-glucosidase inhibitory activities and were also non-cytotoxic against HDF cells. Moreover, the most potent compound **9b** was a competitive inhibitor against α-glucosidase; thus, the molecular modeling study was performed in the active site of α-glucosidase. This study permitted us to evaluation of interaction modes of the synthesized compounds in the α-glucosidase active site. Furthermore, molecular dynamic simulations showed that compound **9b** oriented by vertical U-shape structure into the active site from mouth to the bottom and stabilized the enzyme domains by interacting with the interface of domain A and domain B through long lasting non-binding interactions with Phe157, Thr215, His239, and Arg312 which have the significant role for inhibition activity of the mentioned compound. In silico druglikeness/ADME/T studies revealed that the most potent compounds can be druglikeness agents with appropriate ADME properties and toxicity profile when compared with acarbose.

Experimental

Melting points of 4,5-diphenylimidazole-acetamide-1,2,3-triazole **9a**–**9m** were determined with a Kofler hot stage apparatus. ^{1}H and ^{13}C NMR spectra of these derivatives were obtained with a Bruker FT-500, using TMS as an internal standard. IR spectra of the title compounds recoded with a Nicolet Magna FTIR 550 spectrophotometer (KBr disks). Mass spectra for several synthesized compounds were obtained with an Agilent Technology (HP) mass spectrometer operating at an ionization potential of 70 eV. Finally, elemental analysis was performed by an Elementar Analysen system GmbH VarioEL CHN mode. Compounds **8a**–**8m** were obtained in situ according to described pathway in our previous work [17].

4,5-Diphenyl-2-[4-(prop-2-ynyloxy)phenyl]-1*H*-imidazole (4, $C_{24}H_{18}N_2O$) A mixture of 4-(prop-2-yn-1-yloxy) benzaldehyde (**1**, 1 mmol), benzil (**2**, 1 mmol), and ammonium acetate (**3**, 10 mmol) in 10 cm^3 acetic acid was heated at reflux for 1 h. Upon completion of the reaction (checked by TLC), the obtained mixture was poured into cold water, the precipitate was filtered off, and washed with cold water to afford desired product **4**. White powder; yield: 85%; m.p.: 203–205 °C; IR (KBr): $\overline{\nu}$ = 3417, 3329, 3068 cm^{-1}; ^{1}H NMR (300 MHz, DMSO-d_6): δ = 3.61 (s, 1H, CH), 4.87 (s, 2H, CH_2), 7.11 (d, J = 7.56 Hz, 2H, H2, H6), 7.26–7.37 (m, 6H, Ph), 7.52–7.54 (m, 4H, Ph), 8.02 (d, J = 8.13 Hz, 2H, H3, H5), 11.99 (s, 1H, NH) ppm; ^{13}C NMR (75 MHz, DMSO-d_6): δ = 55.97, 78.80, 115.47, 115.76, 124.29, 127.12, 128.85, 145.96, 157.82, 172.51 ppm; MS (70 eV): m/z = 350 (M^+).

General procedure for the synthesis of 4,5-diphenylimidazole-1,2,3-triazole-acetamide hybrids 9a–9m

A mixture of 4,5-diphenyl-2-[4-(prop-2-ynyloxy)phenyl]-1*H*-imidazole (**4**, 1 mmol), $CuSO_4{\cdot}5H_2O$ (7 mol%), and catalytic amounts of sodium ascorbate was added to the freshly prepared azide derivatives **8a**–**8m** and stirred at room temperature for 18–22 h. Upon completion of the reaction (monitored by TLC), the obtained mixture was poured into crushed ice. After that, the precipitates were filtered off,

washed with water, and purified by recrystallization from ethanol to give the target derivatives **9a**–**9m**.

2-[4-[[4-(4,5-Diphenyl-1*H*-imidazol-2-yl)phenoxy]methyl]-1*H*-1,2,3-triazol-1-yl]-*N*-phenylacetamide (9a, $C_{32}H_{26}N_6O_2$) White powder; yield: 75%; m.p.: 192–194 °C; IR (KBr): $\overline{\nu}$ = 3419, 3062, 1692 cm^{-1}; ^1H NMR (500 MHz, DMSO-d_6): δ = 5.24 (s, 2H, CH_2), 5.36 (s, 2H, CH_2), 7.07 (t, J = 7.5 Hz, 1H, H4′), 7.17 (d, J = 8.9 Hz, 2H, H2, H6), 7.28–7.36 (m, 8H, Ph, H3′, H5′), 7.50–7.51 (m, 4H, Ph), 7.57 (d, 2H, J = 8.5 Hz, H2′, H6′), 8.02 (d, J = 9 Hz, 2H, H3, H5), 8.25 (s, 1H, triazole), 10.47 (s, 1H, NH), 12.65 (s, 1H, NH) ppm; ^{13}C NMR (500 MHz, DMSO-d_6): δ = 52.4, 61.6, 115.3, 123.9, 126.7, 127.2, 127.5, 127.9, 128.8, 139.2, 142.8, 146.0, 158.7, 165.7 ppm; MS (70 eV): m/z = 526 (M^+).

2-[4-[[4-(4,5-Diphenyl-1*H*-imidazol-2-yl)phenoxy]methyl]-1*H*-1,2,3-triazol-1-yl]-*N*-(*p*-tolyl)acetamide (9b, $C_{33}H_{28}N_6O_2$) White powder; yield: 77%; m.p.: 199–201 °C; IR (KBr): $\overline{\nu}$ = 3417, 3065, 1689 cm^{-1}; ^1H NMR (500 MHz, DMSO-d_6): δ = 2.1 (s, 3H, CH_3), 5.20 (s, 2H, CH_2), 5.35 (s, 2H, CH_2), 7.12 (d, J = 8 Hz, 2H, H2, H6), 7.15 (d, J = 8.5 Hz, 2H, H3′, H5′), 7.25–7.45 (m, 7H, Ph), 7.5 (d, J = 7.5 Hz, 2H, H2′, H6′), 7.55 (m, 3H, Ph), 8.05 (d, J = 8.5 Hz, 2H, H3, H5), 8.3 (1H, s, triazole), 10.5 (1H, s, NH), 12.5 (1H, bs, NH) ppm; ^{13}C NMR (500 MHz, DMSO-d_6): δ = 21.0, 52.7, 61.6, 115.3, 119.7, 123.9, 126.8, 127.2, 129.7, 133.2, 136.4, 142.9, 158.7, 164.4 ppm; MS (70 eV): m/z = 540 (M^+).

***N*-(2-Bromo-4-methylphenyl)-2-[4-[[4-(4,5-diphenyl-1*H*-imidazol-2-yl)phenoxy]methyl]-1*H*-1,2,3-triazol-1-yl]acetamide (9c, $C_{33}H_{27}BrN_6O_2$)** White powder; yield: 79%; m.p.: 209–211 °C; IR (KBr): $\overline{\nu}$ = 3419, 3068, 1685 cm^{-1}; ^1H NMR (500 MHz, DMSO-d_6): δ = 2.29 (s, 3H, CH_3), 5.26 (s, 2H, CH_2), 5.45 (s, 2H, CH_2), 7.1–7.20 (m, 3H, H2, H6, H5′), 7.25–7.40 (m, 6H, H3′, Ph), 7.5–7.6 (m, 6H, H6′, Ph) 8.05 (d, J = 8.5 Hz, 2H, H3, H5), 8.3 (s, 1H, triazole), 10.01 (s, 1H, NH), 12.5 (bs, 1H, NH) ppm; ^{13}C NMR (500 MHz, DMSO-d_6): δ = 20.5, 52.4, 61.6, 115.3, 118.1, 123.9, 126.8,127.2, 129.3, 133.2, 133.3, 137.8, 142.8, 146.0, 158.7, 165.2 ppm.

2-[4-[[4-(4,5-Diphenyl-1*H*-imidazol-2-yl)phenoxy]methyl]-1*H*-1,2,3-triazol-1-yl]-*N*-(4-methoxyphenyl)acetamide (9d, $C_{33}H_{28}N_6O_3$) White powder; yield: 75%; m.p.: 202–204 °C; IR (KBr): $\overline{\nu}$ = 3421, 3063, 1681 cm^{-1}; ^1H NMR (500 MHz, DMSO-d_6): δ = 3.73 (s, 3H, OCH_3), 5.24 (s, 2H, CH_2), 5.36 (s, 2H, CH_2), 6.92 (d, J = 8.5 Hz, 2H, H3′, H5′), 7.20 (d, J = 8.5 Hz, 2H, H2, H6), 7.25–7.60 (m, 12H, Ph, H2′, H6′), 8.05 (d, J = 8.5 Hz, 2H, H3, H5), 8.3 (1H, s, triazole), 10.5 (s, 1H, NH), 12.5 (bs, 1H, NH) ppm; ^{13}C NMR (500 MHz, DMSO-d_6): δ = 52.6, 55.6, 61.6, 114.5, 115.3, 121.3, 123.9, 126.8, 127.2, 131.9, 142.8, 146.0, 156.0, 158.7, 164.1 ppm; MS (70 eV): m/z = 556 (M^+).

***N*-(2-Chlorophenyl)-2-[4-[[4-(4,5-diphenyl-1*H*-imidazol-2-yl)phenoxy]methyl]-1*H*-1,2,3-triazol-1-yl]acetamide (9e, $C_{32}H_{25}ClN_6O_2$)** White powder; yield: 72%; m.p.: 184–186 °C; IR (KBr): $\overline{\nu}$ = 3421, 3070, 1684 cm^{-1}; ^1H NMR (500 MHz, DMSO-d_6): δ = 5.20 (s, 2H, CH_2), 5.50 (s, 2H, CH_2), 7.18 (d, J = 9 Hz, 2H, H2, H6), 7.2–7.60 (m, 12H, Ph), 7.75 (d, J = 8 Hz, 1H, H3′), 8.05 (d, J = 8.5 Hz, 2H, H3, H5), 8.3 (s, 1H, triazole), 10.27 (s, 1H, NH), 12.5 (bs, 1H, NH) ppm; ^{13}C NMR (500 MHz, DMSO-d_6): δ = 52.4, 61.6, 115.3, 123.9, 126.9, 126.4, 127.2, 127.5, 128.0, 128.6, 128.8, 129.1, 130.1, 131.7, 134.6, 142.9, 146.0, 158.7, 166.4 ppm.

***N*-(3-Chlorophenyl)-2-[4-[[4-(4,5-diphenyl-1*H*-imidazol-2-yl)phenoxy]methyl]-1*H*-1,2,3-triazol-1-yl]acetamide (9f, $C_{32}H_{25}ClN_6O_2$)** White powder; yield: 72%; m.p.: 206–208 °C; IR (KBr): $\overline{\nu}$ = 3419, 3069, 1684 cm^{-1}; ^1H NMR (500 MHz, DMSO-d_6): δ = 5.25 (s, 2H, CH_2), 5.40 (s, 2H, CH_2), 7.1–7.20 (m, 3H, H4′, H2, H6), 7.3–7.4 (m, 7H, Ph, H3′), 7.50 (d, J = 7.5 Hz, 1H, H6′), 7.55 (m, 4H, Ph), 7.8 (s, 1H, H2′), 8.05 (d, 2H, J = 8.5 Hz, H3, H5), 8.3 (s, 1H, triazole), 10.7 (s, 1H, NH), 12.5 (bs, 1H, NH) ppm; ^{13}C NMR (500 MHz, DMSO-d_6): δ = 52.7, 61.6, 115.3, 118.1, 119.2, 123.9, 124.0, 126.8, 127.2, 128.9, 131.1, 133.7, 140.3, 142.9, 146.0, 158.7, 165.1 ppm.

***N*-(4-Chlorophenyl)-2-[4-[[4-(4,5-diphenyl-1*H*-imidazol-2-yl)phenoxy]methyl]-1*H*-1,2,3-triazol-1-yl]acetamide (9g, $C_{32}H_{25}ClN_6O_2$)** White powder; yield: 68%; m.p.: 185–187 °C; IR (KBr): $\overline{\nu}$ = 3418, 3068, 1687 cm^{-1}; ^1H NMR (500 MHz, DMSO-d_6): δ = 5.25 (s, 2H, CH_2), 5.40 (s, 2H, CH_2), 7.15 (d, J = 9 Hz, 2H, H2,6), 7.2–7.4 (m, 5H, Ph), 7.41 (d, J = 9 Hz, 2H, H3′, H 5′), 7.5–7.6 (m, 5H, Ph), 7.61 (d, J = 9 Hz, 2H, H2′,H6′), 8.10 (d, J = 9 Hz, 2H, H3,H5), 8.3 (s, 1H, triazole), 10.5 (s, 1H, NH), 12.5 (s, 1H, NH) ppm; ^{13}C NMR (500 MHz, DMSO-d_6): δ = 52.7, 61.6, 115.3, 121.3, 123.4, 126.8, 127.2, 127.8, 128.8, 129.3, 137.3, 142.9, 146.0, 158.1, 164.9 ppm.

***N*-(2,3-Dichlorophenyl)-2-[4-[[4-(4,5-diphenyl-1*H*-imidazol-2-yl)phenoxy]methyl]-1*H*-1,2,3-triazol-1-yl]-acetamide (9h, $C_{32}H_{24}Cl_2N_6O_2$)** White powder; yield: 66%; m.p.: 210–212 °C; IR (KBr): $\overline{\nu}$ = 3426, 3071, 1681 cm^{-1}; ^1H NMR (500 MHz, DMSO-d_6): δ = 5.26 (s, 2H, CH_2), 5.50 (s, 2H, CH_2), 7.15 (d, J = 8.5 Hz, 2H, H2, H6), 7.25 (m, 1H, Ph), 7.30 (t, J = 7.5 Hz, 2H, Ph), 7.36–7.40 (m, 2H, Ph), 7.44 (t, J = 7.5 Hz, 2H, Ph), 7.55 (m, 3H, Ph), 7.75 (d, J = 8 Hz, 1H, H6′), 8.05 (d, J = 8.5 Hz, 2H, H3, H5), 8.3 (s, 1H, triazole), 10.27 (s, 1H, NH), 12.5 (bs, 1H,

NH) ppm; ^{13}C NMR (500 MHz, DMSO-d_6): δ = 52.4, 61.6, 115.3, 123.9, 126.8, 127.2, 127.5, 128.1, 128.1, 128.6, 128.8, 129.1, 131.7, 132.5, 135.7, 136.6, 137.3, 142.9, 146.0, 158.7, 165.5 ppm.

***N*-(3,5-Dichlorophenyl)-2-[4-[[4-(4,5-diphenyl-1*H*-imidazol-2-yl)phenoxy]methyl]-1*H*-1,2,3-triazol-1-yl]-acetamide (9i, $C_{32}H_{24}Cl_2N_6O_2$)** White powder; yield: 71%; m.p.: 193–195 °C; IR (KBr): $\overline{\nu}$ = 3424, 3069, 1684 cm^{-1}; ^{1}H NMR (500 MHz, DMSO-d_6): δ = 5.25 (s, 2H, CH_2), 5.40 (s, 2H, CH_2), 7.15 (d, J = 9 Hz, 2H, H2, H6), 7.30–7.55 (m, 11H, Ph, H4′), 7.65 (d, J = 2 Hz, 2H, H2′,6′), 8.05 (d, J = 9 Hz, 2H, H3, H5), 8.3 (s, 1H, triazole), 10.87 (s, 1H, NH), 12.5 (bs, 1H, NH) ppm; ^{13}C NMR (500 MHz, DMSO-d_6): δ = 53.7, 61.6, 115.3, 117.9, 123.6, 123.9, 126.8, 127.2, 134.7, 141.1, 142.9, 146.0, 158.7, 166.5 ppm.

***N*-(3-Chloro-4-fluorophenyl)-2-[4-[[4-(4,5-diphenyl-1*H*-imidazol-2-yl)phenoxy]methyl]-1*H*-1,2,3-triazol-1-yl]acetamide (9j, $C_{32}H_{24}ClFN_6O_2$)** White powder; yield: 67%; m.p.: 196–198 °C; IR (KBr): $\overline{\nu}$ = 3426, 3066, 1683 cm^{-1}; ^{1}H NMR (500 MHz, DMSO-d_6): δ = 5.26 (s, 2H, CH_2), 5.39 (s, 2H, CH_2), 7.15 (d, J = 8.5 Hz, 2H, H2, H6), 7.2–7.6 (m, 10H, Ph), 7.90 (d, J = 7.5 Hz, 1H, H2′), 8.05 (2H, d, J = 9 Hz, H3, H5), 8.3 (s, 1H, triazole), 10.7 (s,1H, NH), 12.5 (s, 1H, NH) ppm; ^{13}C NMR (500 MHz, DMSO-d_6): δ = 52.6, 61.6, 115.3 (d, J = 87.5 Hz), 120.1 (d, J = 28 Hz), 121.2, 123.9, 126.8, 127.2, 142.9, 146.0, 158.7, 165.0 ppm.

***N*-(3-Bromophenyl)-2-[4-[[4-(4,5-diphenyl-1*H*-imidazol-2-yl)phenoxy]methyl]-1*H*-1,2,3-triazol-1-yl]acetamide (9 k, $C_{32}H_{25}BrN_6O_2$)** White powder; yield: 65%; m.p.: 181–183 °C; IR (KBr): $\overline{\nu}$ = 3423, 3066, 1681 cm^{-1}; ^{1}H NMR (500 MHz, DMSO-d_6): δ = 5.30 (s, 2H, CH_2), 5.50 (s, 2H, CH_2), 7.15 (d, J = 9 Hz, 2H, H2, H6), 7.3–7.55 (m, 13H, Ph, H4′, H5′, H6′), 7.95 (1H, s, H2′), 8.05 (2H, d, J = 9 Hz, H3, H5), 8.3 (s, 1H, triazole), 10.6 (s, 1H, NH), 12.5 (bs, 1H, NH) ppm; ^{13}C NMR (500 MHz, DMSO-d_6): δ = 52.7, 61.6, 115.3, 118.5, 122.1, 122.1, 123.9, 126.8, 126.9, 127.2, 131.4, 140.2, 142.9, 146.0, 158.7, 166.1 ppm.

2-[4-[[4-(4,5-Diphenyl-1*H*-imidazol-2-yl)phenoxy]-methyl]-1*H*-1,2,3-triazol-1-yl]-*N*-(2-nitrophenyl)acetamide (9l, $C_{32}H_{25}N_7O_4$) White powder; yield: 69%; m.p.: 218–220 °C; IR (KBr): $\overline{\nu}$ = 3423, 3064, 16,852 cm^{-1}; ^{1}H NMR (500 MHz, DMSO-d_6): δ = 5.26 (s, 2H, CH_2), 5.47 (s, 2H, CH_2), 7.18 (d, J = 8.5 Hz, 2H, H2, H6), 7.2–7.45 (m, 7H, Ph), 7.5–7.55 (m, 4H, Ph, H4′), 7.7–7.9 (2H, m, H3′, H5′), 8.0 (d, J = 8.5 Hz, 1H, H6′), 8.03 (d, J = 8.5 Hz, 2H, H3, H5), 8.3 (s, 1H, triazole), 10.8 (s, 1H, NH), 12.5 (bs, 1H, NH) ppm; ^{13}C NMR (500 MHz, DMSO-d_6): δ = 52.4, 61.5, 115.3, 125.5, 126.0, 126.4, 126.8, 127.2, 130. 8, 134.6, 142.9, 158.7, 165.4 ppm; MS (70 eV): m/z = 571 (M^+).

2-[4-[[4-(4,5-Diphenyl-1*H*-imidazol-2-yl)phenoxy]-methyl]-1*H*-1,2,3-triazol-1-yl]-*N*-(3-phenoxyphenyl)-acetamide (9 m, $C_{38}H_{30}N_6O_3$) White powder; yield: 65%; m.p.: 193–195 °C; IR (KBr): $\overline{\nu}$ = 3423, 3065, 1682 cm^{-1}; ^{1}H NMR (500 MHz, DMSO-d_6): δ = 5.25 (s, 2H, CH_2), 5.36 (s, 2H, CH_2), 6.76 (d, J = 6.5 Hz, 1H, H3′), 7.05 (d, J = 8.5 Hz, 2H, H2, H6), 7.15–7.60 (m, 18H, Ph, H2′, H4′, H5′), 8.05 (d, J = 8.5 Hz, 2H, H3, H5), 8.3 (s, 1H, triazole), 10.50 (s, 1H, NH), 12.5 (bs, 1H, NH) ppm; ^{13}C NMR (500 MHz, DMSO-d_6): δ = 52.7, 61.6, 109.3, 114.2, 114.4, 115.3, 119. 5, 123.9, 124.2, 126.8, 127.2, 127.5, 128.6, 128.7, 128.8, 128.9, 129.1, 130. 6, 130.8, 140.4, 142.7, 146.0, 156. 7, 157.8, 158.7, 164.8 ppm.

α-Glucosidase and α-amylase inhibition assays

In vitro α-glucosidase and α-amylase inhibition assays of compounds **9a**–**9m** were performed according to our previous work [19].

Kinetic studies

Kinetic studies were carried out to determine inhibition mode of standard drug acarbose and the most potent compound **9b**. The 20 mm^3 of enzyme solution (1 U/cm^3) was incubated with different concentrations of acarbose (0, 400, 600, and 800 µM) or compound **9d** (0, 15, 35, and 55 µM) for 15 min at 30 °C. The enzymatic reaction was then started by adding different concentrations of substrate (1–4 mM), and change in absorbance was measured at 405 nm for 20 min using spectrophotometer (Gen5, Power wave xs2, BioTek, America) [20].

Molecular docking study

To find out the interaction modes of the synthesized compounds over the α-glycosidase, Maestro Molecular Modeling platform (version 10.5) by Schrödinger, LLC was performed [21]. There was not any crystallographic structure of *Saccharomyces cerevisiae* α-glucosidase, so the homology modeled structure was constructed using the crystal structure of *S. cerevisiae* isomaltase in complex with α-D-glucose (PDB id: 3A4A) as target structure [22]. The latter enzyme has 72% identical and 85% shares sequence similarity with *S. cerevisiae* α-glucosidase. Despite a small difference in the structures of their active site pockets, such as steric hindrance by two residues, the structure of the active site of α-glucosidase is highly similar to that of isomaltase. Therefore, the active site of α-glucosidase was defined around the location of α-D-glucose after structural superimposing of

α-glucosidase over isomaltase followed by energy minimization and short molecular dynamic to release any undesired strain.

The 2D structures of all synthesized compounds were drawn in Marvin 15.10.12.0 program (http://www.chemaxon.com) and converted into pdb file. The Protein Preparation Wizard and the LigPrep module were used to prepare protein and ligand structures properly [23–25]. The missing side chains of the proteins were filled using the Prime tool and missing residues were updated.

The accurate side-chain and backbone flexibility during ligand binding at the active site of α-glycosidase were predicted by IFD method using Glide software (Schrödinger LLC 2018, USA) [26]. Because the kinetic study of the most potent compound revealed competitive type inhibition mode for this compound, the α-glucosidase active site was used to generate the grid for IFD calculation. The maximum 20 poses with receptor and ligand van der waals radii of 0.7 and 0.5, respectively considered. Residues within 5 Å of the α-D-glucose at the active site were refined followed by side-chain optimization. Structures whose prime energy is more than 30 kcal/mol are eliminated based on extra precious Glide docking.

Molecular dynamic simulation

Molecular dynamic (MD) simulation of this study was performed using the Desmond v5.3 module implemented in Maestro interface (from Schrödinger 2018–4 suite) [30]. The appropriate pose for MD simulation procedure of the compounds was achieved by docking method.

To build the system for MD simulation, the protein–ligand complexes were solvated with SPC explicit water molecules and placed in the center of an orthorhombic box of appropriate size in the Periodic Boundary Condition. Sufficient counter-ions and a 0.15 M solution of NaCl were also utilized to neutralize the system and to simulate the real cellular ionic concentrations, respectively. The MD protocol involved minimization, pre-production, and finally production MD simulation steps. In the minimization procedure, the entire system was allowed to relax for 2500 steps by the steepest descent approach. Then, the temperature of the system was raised from 0 to 300 K with a small force constant on the enzyme to restrict any drastic changes. MD simulations were performed via NPT (constant number of atoms, constant pressure i.e. 1.01325 bar and constant temperature, i.e. 300 K) ensemble. The Nose-Hoover chain method was used as the default thermostat with 1.0-ps interval and Martyna-Tobias-Klein as the default barostat with 2.0-ps interval by applying isotropic coupling style. Long-range electrostatic forces were calculated based on Particle-mesh-based Ewald approach with the he cut-off radius for columbic forces set to 9.0 Å. Finally, the system subjected to produce MD simulations for 20 ns for protein–ligand complex. During the simulation, every 1000 ps of the actual frame was stored. The dynamic behavior and structural changes of the systems were analyzed by the calculation of the root mean square deviation (RMSD) and RMSF. Subsequently, the energy-minimized structure calculated from the equilibrated trajectory system was evaluated for investigation of each ligand–protein complex interaction.

Prime MM-GBSA

The ligand-binding energies (ΔG_{bind}) were calculated for compound **9b** and acarbose using Molecular mechanics/generalized born surface area (MM-GBSA) modules (Schrödinger LLC 2018) (75) based on the following equation:

$$\Delta G_{bind} = E_{complex} - \left[E_{receptor} + E_{ligand}\right],$$

where ΔG_{bind} is the calculated relative free energy which includes both ligand and receptor strain energy. $E_{complex}$ is the MM-GBSA energy of the minimized complex, and E_{ligand} is the MM-GBSA energy of the ligand after removing it from the complex and allowing it to relax. $E_{receptor}$ is the MM-GBSA energy of relaxed protein after separating it from the ligand. The MM-GBSA calculation was performed based on the clustering method for energy calculation.

In vitro cytotoxicity assay

Cytotoxicity evaluation on compounds **9b**, **9d**, and **9h** was performed according to our previous works [19].

In silico druglikeness/ADME/T study

In silico druglikeness/ADME/T studies on compounds **9b**, **9d**, **9h**, and acarbose (standard drug) were performed using the preADMET online server (http://preadmet.bmdrc.org/) [31].

Supplementary Information The online version contains supplementary material available at https://doi.org/10.1007/s00706-021-02779-7.

Acknowledgements This work was financially supported by the National Institute for Medical Research Development (NIMAD) (the grant number: 972514). The ethics code for this study is IR.NIMAD.REC.1398.036 (http://ethics.research.ac.ir/IR.NIMAD.REC.1398.036).

References

1. Saltiel AR (2001) Cell 104:517
2. Yu X, Zhang F, Liu T, Liu Z, Dong Q, Li D (2020) Bioorg Med Chem Lett 30:127528

3. Schmidt DD, Frommer W, Junge B, Müller L, Wingender W, Truscheit E, Schäfer D (1997) Naturwissenschaften 64:535
4. Zhu JH, Zhang DQ, Chen WC (2013) Afr J Tradit Complement Altern Med 10:356
5. Tundis R, Loizzo MR, Menichini F (2010) Mini-Rev Med Chem 10:315
6. Yang CY, Yen YY, Hung KC, Hsu SW, Lan SJ, Lin HC (2019) Nutr Diabetes 9:1
7. Gerber-Lemaire S, Juillerat-Jeanneret L (2006) Mini-Rev Med Chem 6:1043
8. ShnMoorthy N, Ramos MJ, Fernandes PA (2012) Mini-Rev Med Chem 12:713
9. Hackenberg F, Lally G, Müller-Bunz H, Paradisi F, Quaglia D, Streciwilk W, Tacke M (2012) J Organomet Chem 717:123
10. Assadieskandar A, Amini M, Salehi M, Sadeghian H, Alimardani M, Sakhteman A, Nadri H, Shafiee A (2012) Bioorg Med Chem 20:7160
11. Bellina F, Cauteruccio S, Rossi R (2007) Tetrahedron 63:4571
12. Abdellatif KR, Fadaly WA (2017) Bioorg Chem 72:123
13. Yar M, Bajda M, Shahzad S, Ullah N, Gilani MA, Ashraf M, Rauf A, Shaukat A (2015) Bioorg Chem 58:65
14. Naureen S, Chaudhry F, Munawar MA, Ashraf M, Hamid S, Khan MA (2018) Bioorg Chem 76:365
15. Saeedi M, Mohammadi-Khanaposhtani M, Asgari MS, Eghbalnejad N, Imanparast S, Faramarzi MA, Larijani B, Mahdavi M, Akbarzadeh T (2019) Bioorg Med Chem 27:115148
16. Agalave SG, Maujan SR, Pore VS (2011) Chem Asian J 6:2696
17. Asemanipoor N, Mohammadi-Khanaposhtani M, Moradi S, Vahidi M, Asadi M, Faramarzi MA, Mahdavi M, Biglar M, Larijani B, Hamedifar H, Hajimiri MH (2020) Bioorg Chem 95:103482
18. Bakherad Z, Mohammadi-Khanaposhtani M, Sadeghi-Aliabadi H, Rezaei S, Fassihi A, Bakherad M, Rastegar H, Biglar M, Saghaie L, Larijani B, Mahdavi M (2019) J Mol Struct 1192:192
19. Asgari MS, Mohammadi-Khanaposhtani M, Kiani M, Ranjbar PR, Zabihi E, Pourbagher R, Rahimi R, Faramarzi MA, Biglar M, Larijani B, Mahdavi M (2019) Bioorg Chem 92:103206
20. Adib M, Peytam F, Rahmanian-Jazi M, Mohammadi-Khanaposhtani M, Mahernia S, Bijanzadeh HR, Jahani M, Imanparast S, Faramarzi MA, Mahdavi M, Larijani B (2018) New J Chem 42:17268
21. Schrödinger Suite 2018, induced fit docking protocol; Glide version 5.5, S., LLC, New York, NY, 2009; Prime version 2.1, Schrödinger, LLC, New York, NY, 2009
22. Adib M, Peytam F, Rahmanian-Jazi M, Mahernia S, Bijanzadeh HR, Jahani M, Mohammadi-Khanaposhtani M, Imanparast S, Faramarzi MA, Mahdavi M, Larijani B (2018) Eur J Med Chem 155:353
23. ChemAxon Marvin 15.10.12.0 (version number), 2015, ChemAxon http://www.chemaxon.com
24. Schrödinger Release 2018–4: Schrödinger release 2018–4 protein preparation wizard; Epik, Schrödinger, LLC, New York, NY, 2016; Impact, Schrödinger, LLC, New York, NY, 2016; Prime, Schrödinger, LLC, New York, NY, 2019
25. Schrödinger Release 2018–4: LigPrep, Schrödinger, LLC, New York, NY, 2018
26. Schrödinger Release 2018–4: induced fit docking protocol; glide, Schrödinger, LLC, New York, NY, 2018; Prime, Schrödinger, LLC, New York, NY, 2018
27. Yamamoto K, Miyake H, Kusunoki M, Osaki S (2010) FEBS J 277:4205
28. Katsuya Y, Mezaki Y, Kubota M, Matsuura Y (1998) J Mol Biol 281:885
29. Yamamoto K, Miyake H, Kusunoki M, Osaki S (2011) J Biosci Bioeng 112:545
30. Schrödinger Release 2018–4: desmond molecular dynamics system, D. E. Shaw Research, New York, NY, 2018. Maestro-desmond interoperability tools, Schrödinger, New York, NY, 2018
31. Seoul, South Corea: bioinformatics and molecular design research center; 2004. PreADMET program. Available from: URL: http://preadmet.bmdrc.org

Authors and Affiliations

Nima Sepehri[1] · Homa Azizian[2] · Reza Ghadimi[3] · Fahimeh Abedinifar[4] · Somayeh Mojtabavi[5] · Mohammad Ali Faramarzi[5] · Ali Akbar Moghadamnia[6] · Ebrahim Zabihi[6] · Gholamhossein Mohebbi[7] · Bagher Larijani[4] · Haleh Hamedifar[8] · Maryam Mohammadi-Khanaposhtani[6] · Mohammad Mahdavi[4]

1 Nano Alvand Company, Avicenna Tech Park, Tehran University of Medical Sciences, Tehran, Iran

2 Department of Medicinal Chemistry, School of Pharmacy, Iran University of Medical Sciences, Tehran, Iran

3 Social Determinants of Health Research Center, Health Research Institute, Babol University of Medical Sciences, Babol, Iran

4 Endocrinology and Metabolism Research Center, Endocrinology and Metabolism Clinical Sciences Institute, Tehran University of Medical Sciences, Tehran, Iran

5 Department of Pharmaceutical Biotechnology, Faculty of Pharmacy, Tehran University of Medical Sciences, Tehran, Iran

6 Cellular and Molecular Biology Research Center, Health Research Institute, Babol University of Medical Sciences, Babol, Iran

7 The Persian Gulf Marine Biotechnology Research Center, The Persian Gulf Biomedical Sciences Research Institute, Bushehr University of Medical Sciences, Bushehr, Iran

8 CinnaGen Medical Biotechnology Research Center, Alborz University of Medical Sciences, Karaj, Iran